Analysis of Hook Formation Mechanism in Ultra Low Carbon Steel using CON1D Heat Flow – Solidification Model

Ho-Jung Shin[1], Brian G. Thomas[2], Go-Gi Lee[1], Je-Min Park[3], Chang-Hyun Lee[3], and Seon-Hyo Kim[1]

[1] Department of Materials Science and Engineering, Pohang University of Science and Technology; Pohang, Kyoungbuk, 790-784, South Korea
[2] Department of Mechanical and Industrial Engineering, University of Illinois at Urbana-Champaign; 1206 West Green St., Urbana, IL 61801, USA
[3] POSCO / Steelmaking department / Technology Development Group, Gwangyang Works, Gwangyang, Jeonnam, 545-711, South Korea

Keywords: Ultra low carbon steel, Continuous casting process, Hook formation, Heat flow, Initial solidification

Abstract

Subsurface hook formation at the meniscus during the continuous casting of steel slabs is an important cause of surface defects, owing to their easy entrapment of mold flux and inclusion-laden gas bubbles. This work investigates the fundamentals of meniscus solidification and how hooks form by a combination of advanced computational models and plant measurements. From experimental results, the pitch deviation of oscillation mark depends on mold level fluctuation so the pitch deviation shows the stability of production conditions. The predicted shell thickness at upper end of the oscillation mark is related to the measured thickness of hook. During hook formation, the initial solidifying shell is partly melted by the molten steel. The extent of melting correlates with the location of the liquidus line near the meniscus for a given set of casting conditions. Thus, shallower hooks also correlate with a thinner initial solidifying shell. Deviations between these predicted hook characteristics and measurements correlate with level fluctuations, as indicated by variations in oscillation mark pitch. This work shows that hook shape is greatly affected by heat flux at the meniscus region.

Introduction

Initial solidification at the meniscus occupies a very short region of the mold but greatly affects the quality of the final steel product. Most slab surface defects, including cracks [1] and slivers [2], originate at the meniscus. Many previous studies have aimed to optimize the many inter-related operation parameters [3-7] which affect surface quality. One of these is heat flux to the mold, particularly at the meniscus [5, 7-9]. Understanding of the underlying fundamentals is incomplete, however. Many conflicting mechanisms have been proposed to explain the formation of oscillation marks, subsurface hooks, and their related surface quality problems which have not been tested with plant measurements.

Subsurface hooks form at the meniscus during the continuous casting of steel slabs and often lead to surface defects such as slivers and pencil-pipe blisters in the final rolled sheet product [2, 5]. This is because they tend to entrap inclusions and bubbles. Many previous studies of surface quality have focused on hook formation mechanism [10-16] and the effect of operation parameters on hooks [6, 9, 17-19]. Ultra-low carbon steels are particularly prone to hook formation [20, 21], perhaps owing to their thin mushy zone [17]. These steels, which are designed for high ductility applications such as automobile exterior panels, also require very high surface slab quality. Therefore it is important to correlate subsurface hooks in ultra-low carbon steels with operation parameters, to improve their surface quality. This work focuses on the effects of meniscus heat flux and level fluctuations on hook formation.

To investigate mold heat flux and initial solidification phenomena, this work combines plant experiments, metallurgical analysis, and computational models. Mold temperature was monitored during the continuous casting of ultra-low carbon steels by embedding thermocouples in the copper mold walls. Meniscus level, casting speed, electromagnetic breaking current, and other conditions were also monitored. Slag layer thickness and surface profiles were measured with nail boards. Oscillation mark and hook characteristics were measured on steel samples collected during each test. The model was calibrated to match the measurements of the total heat removed by the cooling water and the measured thermocouple temperatures. The model and metallurgical results were evaluated together to gain new insights into hook formation.

Experiments

Plant experiments were performed using the conventional parallel-mold continuous slab caster at POSCO Gwangyang Works #2-1 caster during August 2003. To help quantify heat flux profiles in the mold, 32 copper/constantan thermocouples were embedded in the wide face of the copper mold walls to monitor mold temperature. The thermocouples were embedded 22mm beneath the hot face in three different rows located 175 mm, 300 mm and 430 mm below the top of mold. The test heats were all cast close together on the same mold, using the ultra-low carbon steel composition given in Table I, and the mold powder composition and properties given in Table II.

Table I Steel composition of ultra-low carbon steel (wt. %)

C	Mn	Si	P	S	Cr	Ni	Cu	Ti	Al
0.003	0.08	≤ 0.005	~ 0.015	~ 0.01	0.01	0.01	0.01~0.02	0.05	~ 0.04

Table II Mold powder composition and properties

Chemical composition (wt. %)	SiO_2	CaO	MgO	Al_2O_3	TiO_2	Fe_2O_3	MnO_2	P_2O_5	Na_2O	K_2O	F	B_2O_3	Li_2O
	36.7	36.8	1.92	4.85	0.03	0.3	0.04	0.01	3.64	0.01	7.01	1.17	0.87

Properties	Solidif. Temperature (^oC)	Softening Temperature (^oC)	Viscosity (Poise)		
			1200 ^oC	1300 ^oC	1400 ^oC
	1101	1145	5.85	2.62	1.28

Five tests were conducted under the conditions given in Table III and each test lasted for most of one heat. These conditions include variations in casting speed (V_C) and electro-magnetic current. Variations in these two operation conditions were studied because increasing casting speed is known to cause a significant increase in heat extraction at the meniscus region [8] and increasing electro-magnetic current is reported to induce high meniscus temperature [22]. Other parameters affecting heat flux in the mold, such as steel grade [8, 23, 24], mold powder [8, 23], and mold plate thickness [8, 9], were kept constant. During casting under stable conditions, a nail board test was conducted for each heat. In these tests, boards with 14-20 pairs of stainless steel and aluminum (Al) wires, were dipped into the top of the mold for 3~4 seconds to measure the steel surface and slag pool depth .

Many operation parameters were recorded once per second, including metal level, mold thermocouple temperatures, cooling temperature at inlet and outlet, and flow rate of the cooling water which were used to quantify heat flux. Once during each heat, a 100-mm long portion of the slab length was collected when conditions were stable. Hook and oscillation mark characteristics were measured on the narrow face of each slab sample to analyze slab surface quality. Oscillation mark pitch, width and depth were measured for ~ 200 oscillation mark profiles using a laser-based surface profilometer along 21 different lines down the narrow face. The narrow-face samples were then sectioned at 5 different distances between the wide faces and etched for metallographic analysis. Hook characteristics were measured for 22 ~ 47 hooks for each test condition.

Table III Test casting conditions

	Casting speed (m/min)	Electro-magnetic Current (A)	Tundish Temperature (^{o} C)	Slab width (mm)	Oscillation stroke (mm)	Oscillation frequency (cpm)	Mean level fluctuation (entire heat) (mm)	Mean level fluctuation (during sampling) (mm)
Heat 1	1.75	313	1560	1300	7.5	187	0.72	0.66
Heat 2	1.42	234	1564	1300	6.8	155	0.71	0.47
Heat 3	1.22	0	1564	1300	6.4	135	0.82	0.46
Heat 4	1.47	277	1571	1570	6.9	159	0.85	0.71
Heat 5	1.47	0	1567	1570	6.9	160	0.77	0.62

Level fluctuations

Mean level fluctuations were computed by taking the standard deviation of the raw Eddy-current level sensor signal. Table III shows two different values for each test heat, based on averaging over 1) the entire heat, and 2) just the 45-second time interval near when the slab samples were cast. The signals for the latter measurements are shown in Figure 1.

No particular trend can be seen for the effect of operating conditions on level fluctuations. However, random events appear to have caused significant differences between the level fluctuations occurring during the short time of sample production, which has important consequences on oscillation mark pitch and surface quality discussed later.

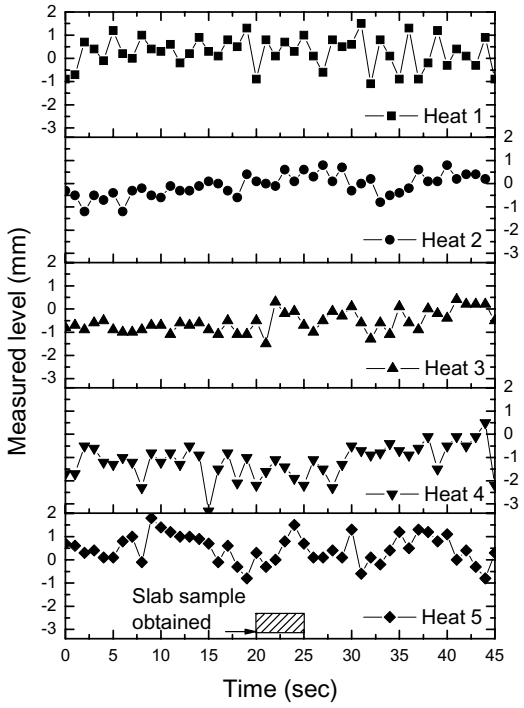

Figure 1 Measured level fluctuation during obtaining slab samples

Nail board tests

For each heat in the plant trials, a nail board test was conducted to determine the mold slag depth, steel surface profile, flow direction and flow velocity. Each nail board had 14-20 pairs of stainless steel and aluminum wires and was held beneath the top surface of the mold for 3-4s. From the difference between the lengths of each pair wires after the test, the slag pool thickness can be estimated given in Table IV, Values for each quarter of the mold surface were obtained by averaging the measurements of 6 ~10 wires. An example is given in Fig. 2 a), which also shows the flow direction and surface velocities estimated from the slope of the steel lump that solidifies onto the bottom of each steel wire. The steel surface profile and the average distance from the top of the mold are also estimated from this test. The metal level decreases with higher casting speed, which agrees with previous work [23].

The results in Fig. 2 b) and Table IV show that the steel level in the mold is lifted higher at the narrow face, owing to the classic double-roll flow pattern in the mold. This flow pattern is confirmed by the surface velocities in Fig. 2 a), which are generally directed from the narrow face toward the SEN. The surface level naturally slopes downward from the narrow face towards the SEN (Fig. 2 b)). This slope generally becomes steeper with increasing casting speed, or without electromagnetic braking. These expected results show the power of the nail-board experiments in monitoring the slag layer, steel surface shape and flow conditions, as proposed by Thomas [25].

Table IV Mean values of nail board tests

	Slag layer thickness (mm)		Steel surface location from top of the mold (mm)	
	Near narrow face	Near SEN	Near narrow face	Near SEN
Heat 1	15.5	13.4	124.0	126.3
Heat 2	9.9	9.2	103.9	104.0
Heat 3	14.2	23.3	98.8	118.4
Heat 4	12.7	10.8	113.8	122.2
Heat 5	10.8	11.8	113.4	138.5

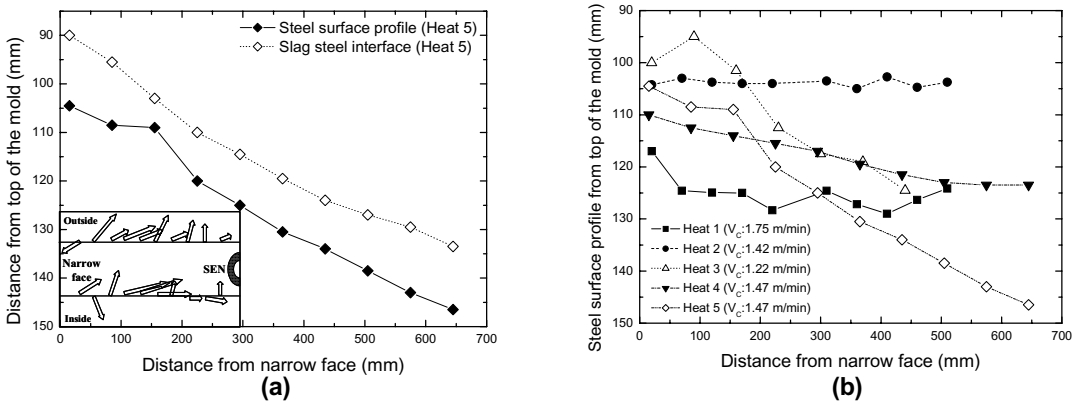

Figure 2 Measured mold slag layer depth, steel surface profile, flow direction and flow velocity

Oscillation mark measurements

Before measurement of the oscillation mark profile, each of the five test samples was sand-blasted to remove any scale from the surface. Oscillation mark pitch, width, upper width, and depth were measured along an 80-mm length of the narrow face (8~9 oscillation marks) using a profilometer. Mean results (Table V) were obtained by averaging across the slab thickness (230 mm) at 21 places (10 mm increments). Figure 3 shows an example oscillation mark and its measured profile. The theoretical oscillation mark pitch is found from the casting speed divided by the oscillation frequency.

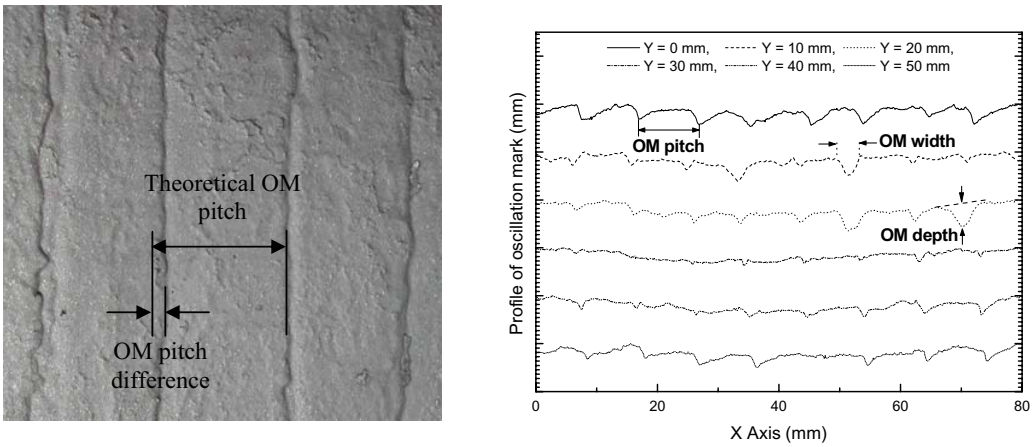

Figure 3 Example of oscillation mark and profile measurement

Hook characteristic measurements

After measuring the oscillation marks, five sections along the narrow face of each of the 5 test samples were cut for hook analysis. After polishing to 0.25 μm, the sections were etched for ~45 minutes with a special picric acid solution. Hook characteristics were then measured near each of the 43~49 oscillation marks observed. Statistics tabulated in Table V were compiled by averaging the measurements obtained for the 22 ~47 hooks that were found in each test sample.

The hook characteristics defined for this study were hook depth, hook length, hook angle and hook shell thickness, as illustrated in Figure 4. The hook definitions here are based on the hook starting as an initial solidifying shell at the meniscus region, which later curves away from the mold wall. As pictured in Fig. 4, each hook has an internal line, assumed to be the original surface. Dendrites often grow in both directions from this line. Those growing toward the molten steel indicate the

hook shell thickness while it was solidifying. Those growing towards the upper left likely occurred after the hook was overflowed with new liquid metal. Traces of entrapped mold powder are often observed on the lower right side of the hook.

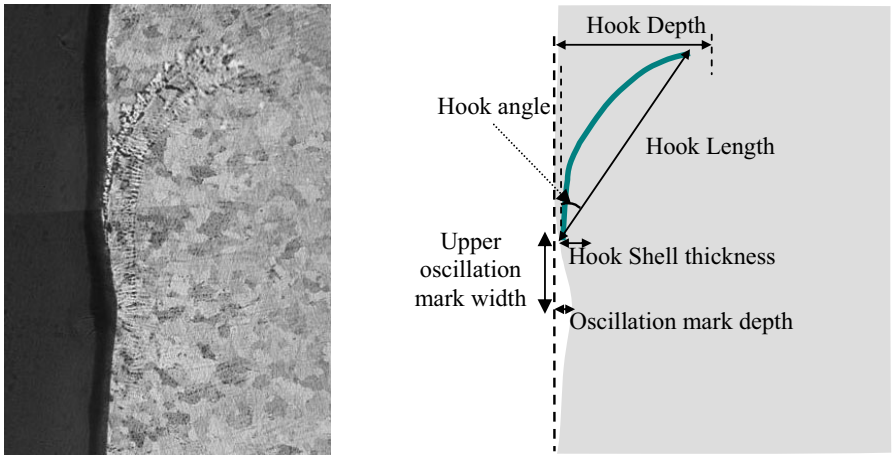

Figure 4 Example of hook and definition of its characteristics

The hook depth is defined in this work as distance from the slab surface up to furthest inner extent of the hook, as pictured in Fig. 4. This parameter is of practical importance, and has been measured by many others [9, 21, 26], because it indicates the thickness of surface layer that should be removed during grinding to completely eliminate the hook and its associated inclusions. This definition differs from that of Kitano et al. [20], which considered only the perpendicular distance from the oscillation mark root to the end of the hook internal line.

The hook length is defined as the linear distance from the starting point of the hook internal line on the shell surface near the upper end of the oscillation mark to its end point. This concept is similar to measurements by Pütz et al. [27]. The hook angle is derived from the depth and length and indicates how much the hook bends away from the mold. Finally, hook shell thickness is measured at the starting point of the hook near the upper end of the oscillation mark, which generally represents the thickest part of the hook. The "upper-width" of the oscillation mark is the distance measured from the deepest part of the oscillation mark to its upper end point, where the surface becomes reasonably flat and the hook thickness is usually measured. Hook shell thickness is a new concept not measured in previous work. It is believed to indicate the heat flux conditions present at the meniscus during formation of the hook. The measurement location at the upper end of the oscillation mark is carefully chosen to allow comparison with model predictions of hook shell thickness.

Table V Mean value of oscillation mark and hook characteristics

	Theoretical pitch of OM (mm)	Measured OM pitch (mm)	Measured OM width (mm)	Measured OM depth (mm)	Measured hook depth (mm)	Measured hook length (mm)	Measured hook angle (mm)	Measured hook shell thickness (mm)
Heat 1	9.35	9.44	6.12	0.251	1.11	1.92	27.0	0.462
Heat 2	9.16	9.10	6.76	0.328	1.22	1.76	30.9	0.520
Heat 3	9.00	8.91	6.66	0.280	1.29	1.60	34.6	0.268
Heat 4	9.20	9.36	6.29	0.314	1.21	1.83	26.1	0.347
Heat 5	9.19	9.09	6.57	0.272	1.06	1.65	28.0	0.236

Computational Model: CON1D

A computational model, CON1D, was applied to study initial solidification, heat transfer and hook formation at the meniscus. The model features a 1-D transient finite-difference calculation of heat conduction within the solidifying shell coupled with 2-D steady state heat conduction [28]. It includes a simple analytical model of microsegregation for the solidification of multi-component steel alloys from Won et al [29]. Based on previous validation work [28], the model is shown to reproduce temperatures, shell thickness, and interface parameters in the mold region. The application in this work to the meniscus region is only a crude preliminary study because axial heat conduction and undercooling effects are ignored.

The model input conditions were chosen to match the 5 sets of plant operating conditions given in Table III, and also include the steel composition in Table I, mold powder composition in Table II, meniscus location and slag pool thickness from Table IV, and measured oscillation mark shape in Table V. The viscosity of the molten slag, $\mu\,(T)$ is assumed to vary exponentially with temperature:

$$\mu = \mu_o \left(\frac{T_o - T_{fsol}}{T - T_{fsol}} \right)^n \qquad [1]$$

where T_{fsol} is the solidification temperature and μ_o is the viscosity at T_o (1300 °C) taken from Table II and the viscosity exponent n is chosen as 1.15 to best fit the viscosity data in Table II [27]. Figure 5 compares Eq. [1] with the measured viscosity data. Viscosity increases many orders of magnitude with decreasing temperature towards the solidification temperature [30].

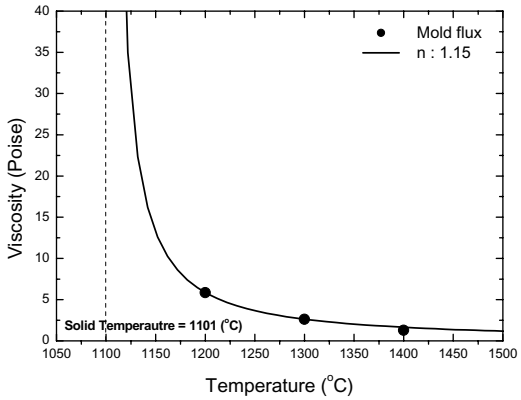

Figure 5 Exponent for temperature dependency of viscosity

The CON1D model imposes a mass balance to express the fact that the input powder consumption must equal the total powder flow rate past every location down the interfacial gap, as shown Figure 6. The following equation expresses the balance of the total consumption, Q_f (kg/m^2) as the density was assumed constant density (2.7 *g/ml*):

$$\frac{Q_f V_C}{\rho_{flux}} = V_S d_S + V_l d_l + V_C d_{OSC} \qquad [2]$$

where the average depth of the oscillation marks (relative to their volume to carry flux), d_{OSC}, is calculated from the volume of the oscillation mark (width x depth)/2 divided by the theoretical oscillation mark pitch.

In general, the mold powder consumption rate should be calculated from the weight of the bags consumed during an entire sequence. Lacking this information, the local mold powder consumption rates were estimated for the conditions of each test sample and are given in Table VI. The flux carried in the oscillation marks, which is the last term in Eq. 2, was calculated from the measured depth, width and pitch of the oscillation marks in Table V. The total local consumption rate input to CON1D must be larger than the consumption rate carried in the oscillation marks. Minor changes to the total consumption rate were made during model calibration in order to match the mean heat flux and measured thermocouple temperatures, as discussed in the next section. The graph of Figure 6 compares the powder consumption rates carried in the oscillation marks with the consumption rate after calibration. The trend clearly shows that the oscillation marks are responsible for most of the flux consumption [31].

Table VI Powder consumption rate carried with OM and inputted to CON1D

	Flux consumption carried in measured OM volume (kg/m^2)	Powder consumption rate input to CON1D (kg/m^2)	Constant ratio of solid flux velocity to casting speed input to CON1D
Heat 1	0.213	0.318	0.03
Heat 2	0.338	0.385	0.0001
Heat 3	0.288	0.341	0.01
Heat 4	0.283	0.347	0.0001
Heat 5	0.253	0.334	0.021

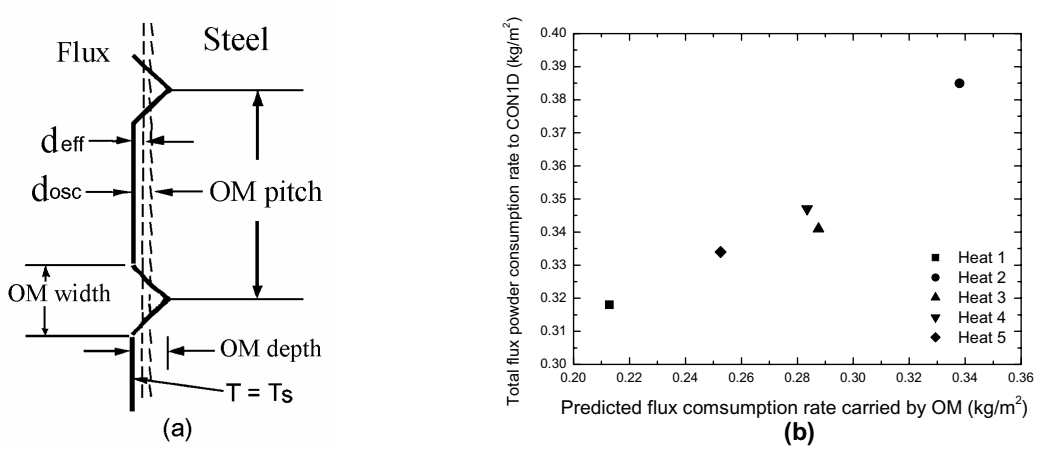

Figure 6 a) Model treatment of oscillation marks (OM) in CON1D and b) flux consumption input data

Model Calibration

The solidification model, CON1D, was calibrated by matching it simultaneously with measurements of total heat extraction from the mold, based on the cooling water temperature difference, and with the thermocouple measurements.

Calibration with Cooling-Water Temperature Rise

The first step of model calibration was to match with the mean heat flux measured in the mold. The mean heat flux in the mold was determined from the temperature difference between the inlet and outlet cooling water and the cooling water flow rate. This was accomplished by varying model parameters such as the mold powder consumption rate and solid flux velocity until the predicted cooling water temperature difference matched the measured value, given in Table VII. Table VII also shows the measured mean heat flux and the value calculated by CON1D. Although both were obtained with same equation, the deviations are caused by differences in the working mold length. The measured mean heat flux recorded at the plant was based on a fixed value (800mm), but the calculated value from CON1D was found by deducting the meniscus level measured from the steel wire length in the nail board test (Table IV) from the total mold length (900mm). This produces minor variations for some tests. The CON1D values should be more accurate.

Table VII Differences of cooling water temperature and mean heat flux

	Working mold length (mm)	Measured ΔT (^oC)	Calculated ΔT (^oC)	Measured mean heat flux (kW/m^2)	Calculated mean heat flux (kW/m^2)
Heat 1	775	6.75	6.75	1666	1709
Heat 2	796	5.78	5.79	1429	1426
Heat 3	790	5.72	5.71	1413	1417
Heat 4	782	7.08	7.08	1430	1449
Heat 5	774	7.49	7.49	1516	1551

Calibration with Mold Temperature

The first step of calibration with the single value of cooling water temperature rise over the entire mold is not sufficient to determine an accurate heat flux profile down the mold, that is needed for the study of initial solidification. To further calibrate the model, its parameters were further adjusted to match the average temperatures measured by the three rows of thermocouples in the wide face for each test heat. The thermocouple locations below meniscus are given in Table VIII, which takes into account the measured variation in meniscus level in the mold for each heat. Thermocouple temperatures were measured every second like other operation parameters and were averaged over a long time of stable casting for each test heat [32]. Computed thermocouple temperatures were based on an offset of 7 mm, to account for the difference between the true three-dimensional temperature profile in the mold wall and the simplified mold temperature equations in CON1D [33].

Table VIII Distance of thermocouple location below meniscus

	1st thermocouple location (mm)	2nd thermocouple location (mm)	3rd thermocouple location (mm)
Heat 1	49.9	174.9	304.9
Heat 2	71.0	196.0	326.0
Heat 3	65.0	190.0	320.0
Heat 4	57.0	182.0	312.0
Heat 5	49.1	174.1	304.1

Table IX Mean temperature from mold thermocouples

	1st thermocouple temperature (°C)		2nd thermocouple temperature (°C)		3rd thermocouple temperature (°C)	
	Measured	Calculated	Measured	Calculated	Measured	Calculated
Heat 1	173.8	185.2	126.2	140.3	115.7	121.0
Heat 2	160.1	159.3	128.9	118.7	109.7	102.9
Heat 3	149.3	158.4	113.8	116.1	102.6	100.1
Heat 4	162.6	169.5	133.2	123.3	113.3	105.8
Heat 5	159.7	173.3	129.0	127.0	112.0	108.6

In order to calibrate the model to match both the total heat flux and the thermocouple temperatures in Table IX, total consumption rate of mold flux and the ratio of solid flux velocity to casting speed were both adjusted for each test heat. Although the consumption rate could be measured on average, local variations are expected due to local changes in the oscillation marks. Thus, this parameter was selected as a calibration parameter. Solid flux velocity ratio is another parameter that is difficult to measure, but greatly affects mold heat transfer [34]. Increasing consumption rate lowers heat flux, especially in the meniscus region. Increasing solid flux velocity increases heat flux, especially lower in the mold. By changing both together, the shape of the heat flux curve was altered to match the thermocouple measurements for each of the 5 tests, while maintaining the total heat flux values given in Table VII. Figure 7 shows the predicted mold temperatures at the depth of the thermocouples near the cold face, compared with the measurements, for a typical test.

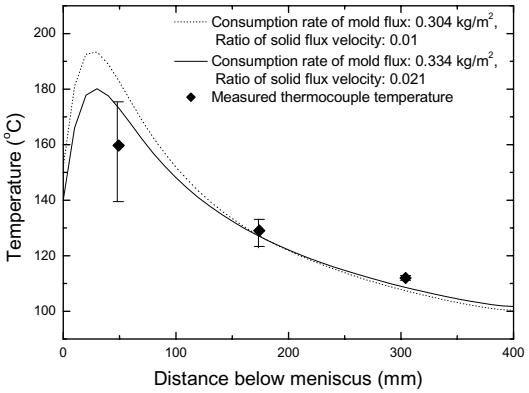

Figure 7 Example of measured and predicted mold temperature profiles (Heat 5)

Model Predictions

Heat flux

Heat flux profiles down the mold were obtained from the calibrated CON1D simulations for each test heat, as shown in Figure 8. Heat flux generally increases with increasing casting speed [8], which corresponds to the trend of the measured mean heat flux. The initial heat flux profile near the meniscus, of most concern in this work, reaches very high values. Thermocouples are unable to capture these peaks.

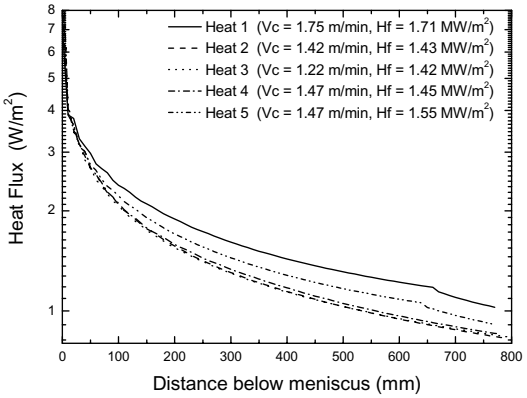

Figure 8 Heat flux profiles predicted by CON1D model

Shell thickness

Shell thickness profiles down the mold are compared for each test in Figure 9. The shell thickness at mold exit is observed to decrease with increasing casting speed, as expected [8, 35]. A close-up at the meniscus region is shown in Figure 9 b). The profiles of the first oscillation mark below the meniscus are also shown for each test. Although the effect of oscillation marks is included in the model, the effect of individual marks on localized shell thinning is not. This effect can be important in the meniscus region of interest in this study. Thus, only the shell thickness predictions between the meniscus and the top of the oscillation mark (~6.5mm below the meniscus) will be compared later with hook shell thickness measurements.

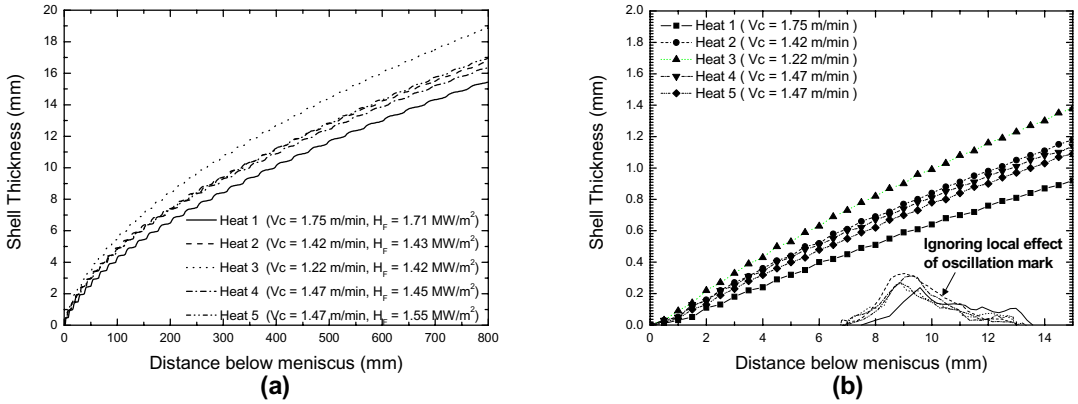

Figure 9 Shell thickness predictions (0.8 solid fraction)

Shell temperature

Shell surface temperature predictions, shown in Figure 10, are complicated to explain. Shell temperature depends on both casting speed and heat flux, which varies down the mold with many parameters including oscillation mark shape, flux consumption rate, solid-flux velocity ratio. Thus no trend shows with casting speed or mean heat flux. For the same casting speed (Heat 4 and 5), higher heat flux has higher shell temperature.

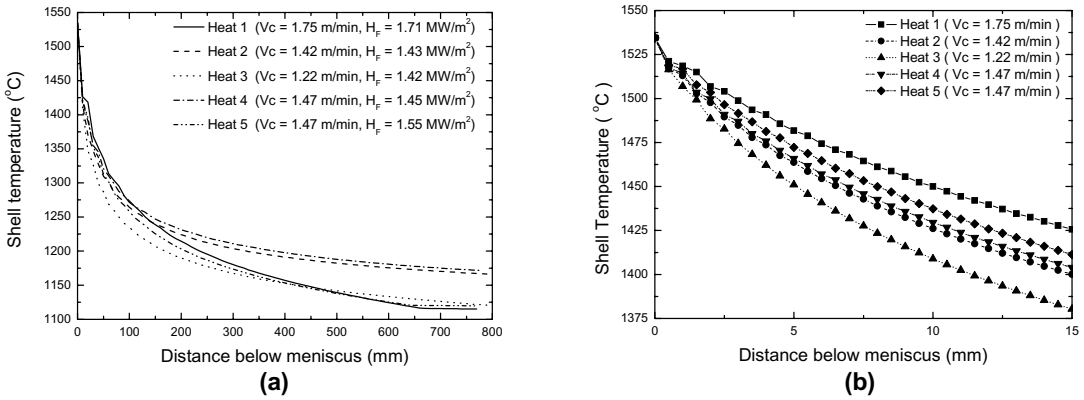

Figure 10 Shell surface temperature predictions

Results Analysis

Effect of level fluctuations on oscillation mark pitch

Figure 11 a) shows the deviation of mean oscillation mark pitch around the strand perimeter for two extreme cases (Heat 3 and 4). Increasing pitch deviations indicates casting during more severe level fluctuations [36]. Even in static-cast ingots which have no oscillation, surface waves on the liquid metal during mold filling cause surface marks [37]. The effect of the measured level fluctuations on the local oscillation mark pitch is shown in Figure 11 b). The standard deviation of oscillation mark pitch was obtained from the difference between each measured oscillation mark pitch and the theoretical oscillation mark pitch, considering ~ 200 oscillation marks per test. This figure shows a clear trend, in spite of a lack of relationship between level fluctuations and operation parameters (see Table III). Greater level fluctuations cause larger standard deviation of oscillation mark pitch. This finding shows that the operating stability and level fluctuations can be predicted from the distribution of oscillation mark pitch.

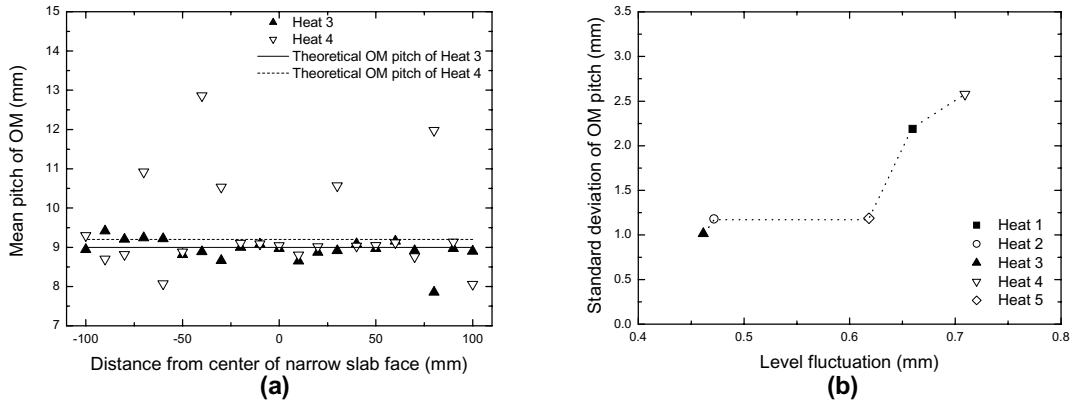

Figure 11 Oscillation mark pitch a) distribution around strand perimeter and b) effect of level fluctuation

Hook shell thickness prediction

To interpret and understand initial solidification behavior, model analysis and experimental hook results were linked. As previously discussed, the thickness profile of the hook is suspected to contain information regarding heat flux at the meniscus when it formed. The measured hook shell thickness and other characteristics were compared with CON1D shell thickness predictions in the meniscus region.

Figure 12 shows a typical hook and a graph of hook shell thickness profile, compared with the CON1D prediction of the shell thickness profile near the meniscus. For the calculation, the meniscus location where the hook shell starts is taken at one theoretical oscillation mark pitch above the measured deepest part of the oscillation mark at the hook. This suggests that the etched hook shape was created by a change in heat flow conditions that occurred due to metal overflow of the initial shell at the meniscus at the instant that the oscillation mark formed. The predicted shell profile roughly matches the measured profile, assuming that the top of the actual hook shell was truncated, likely due to melting during the liquid overflow event.

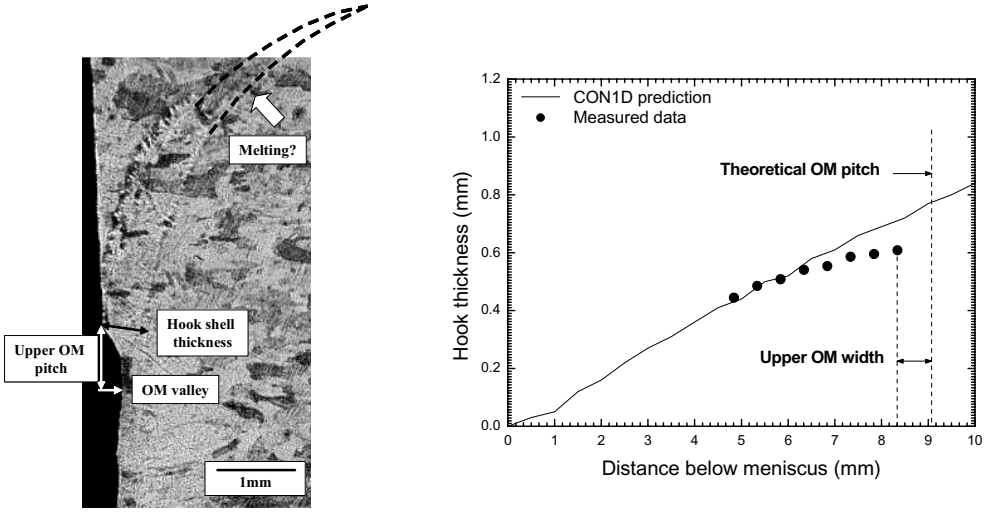

Figure 12 Typical hook shape matching to shell thickness prediction from CON1D (Heat 2)

To further investigate this mechanism, the CON1D model results for the 5 test heats were compared with the measured hook shell thicknesses. The hook shell thickness was measured at the upper end of the oscillation mark where the hook starts (Figure 4). To orient this position relative to the meniscus in the CON1D prediction, the measured upper width of the oscillation mark was subtracted from the pitch. Thus, the measured hook shell thickness typically corresponds with the predicted shell thickness around 7 mm below the meniscus. Table X shows the measured upper width of the oscillation marks for each test. Figure 13 a) compares the measured hook shell thickness with predicted shell thickness based on the mean width of the upper oscillation mark. The mean of the measured hook shell thicknesses for each test matches the prediction remarkably well. The large deviations indicate the variation in hook shells, caused in part by variations in the oscillation mark width.

To further investigate the accuracy of the prediction, maximum and minimum hook shell thicknesses were predicted, based on assuming that the maximum hook-shell thickness occurs on the hook with the minimum upper-width. The shell thicknesses from CON1D for these corresponding new positions are compared with the measurements in Figure 13 b). The agreement is much stronger. The relationship is very strong, considering the many approximations. This tends to confirm the proposed mechanism regarding hook formation.

Table X Measured upper oscillation mark width from the results with profilometer

	Measured oscillation mark upper width (mm)			Shell thickness from CON1D		
	Mean	Maximum	Minimum	Mean	Maximum	Minimum
Heat 1	2.08	7.40	0.40	0.49	0.6	0.12
Heat 2	2.28	7.80	0.40	0.6	0.7	0.10
Heat 3	2.65	7.80	0.80	0.66	0.84	0.10
Heat 4	2.59	8.60	0.40	0.57	0.74	0.04
Heat 5	2.27	6.20	0.60	0.53	0.67	0.22

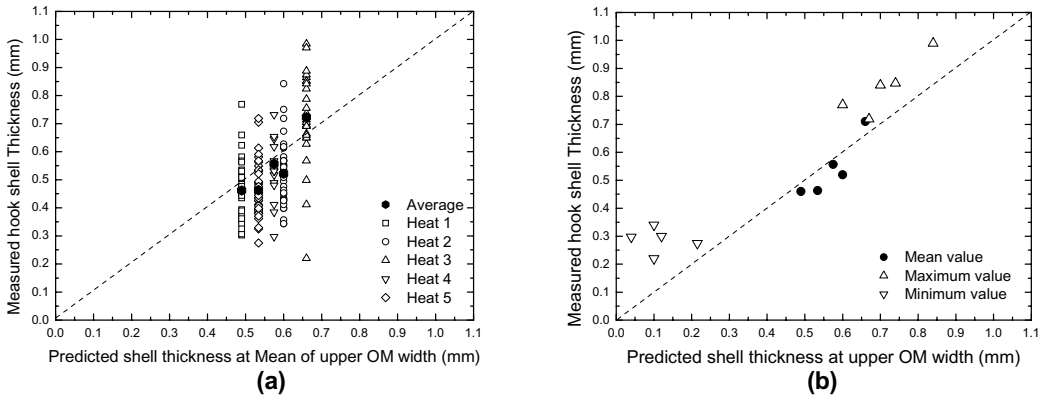

Figure 13 Comparison between measured and predicted shell thickness at upper end of oscillation mark

Effect of hook shell thickness on hook depth

Hook shell thickness and hook length were related to solidus and liquidus line at the meniscus region affected by heat transfer in the mold. Figure 14 shows the relation between measured hook shell thickness and depth, including the results of other related work [38]. Thinner hook shell thickness leads to shallower hooks. The minor deviations may be caused by other phenomena such as oscillation conditions, superheat and level fluctuations.

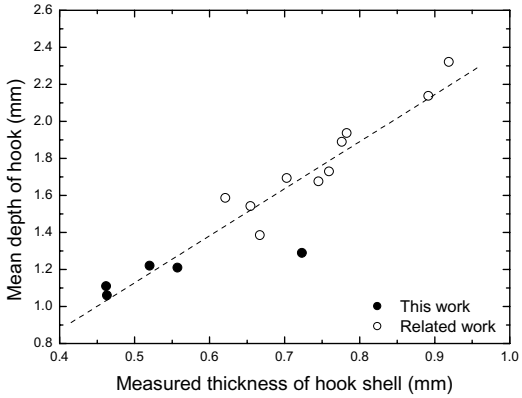

Figure 14 Influence of hook shell thickness on hook depth

Effect of superheat on hook characteristics

Based on the mechanism of hook formation discussed previously, it is expected that superheat should affect the size and extent of hook formation. In contrast with the typical hook structure shown in Figure 12, some oscillation marks show no evidence of a subsurface hook, especially those with high superheat. Figure 15 shows an intermediate case of a "surface hook", consisting of a thin layer running along the surface near the oscillation mark, that is sometimes called a "bent hook" or "bent type with segregation" [9, 39]. Like typical subsurface hooks, the surface hook is often distinguished by thin dark or light bands, due to local segregation. Figure 15 b) shows the effect of superheat on the occurrence rate of hooks and surface-type hooks. The hook occurrence rate was calculated from the total number of hooks (both subsurface and surface) divided by the number of oscillation marks observed (43~49 per data point). Surface hook fraction is the number of surface hooks like those in Fig. 15 a) relative to the total number of hooks observed. Superheat is the temperature difference between the

tundish temperature and the liquidus temperature of the steel composition in Table I, predicted by CON1D. Increasing superheat lowers the hook occurrence rate and increases the fraction of surface hooks. As both effects decrease hook problems, higher superheat is beneficial for surface quality.

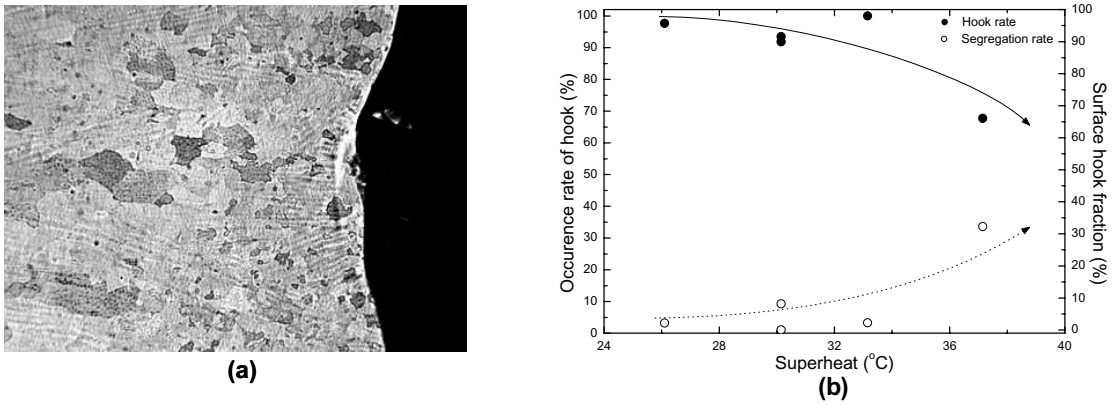

Figure 15 Influence of superheat on hook occurrence rate and hook type

Effect of liquidus line on melting of solidifying shell

Having shown the importance of superheat, further investigations were performed to predict the shortening of hook depth due to melting. Hook shape is usually curved [9, 21, 25, 39]. Many previous works have tried to explain hook curvature due to bending [10. 17, 40, 41], sub-meniscus [13], solidification [14-16] and /or thermal distortion [42] of the initial solidifying shell. It was assumed here that the initial solidification shell in Figure 9 b) bends to the measured hook angle in Table V. The extended shell is then assumed to melt off where it crosses with the corresponding liquidus line predicted by CON1D in Figure 16 a). Figure 16 b) illustrates an example bent shell and its truncated length.

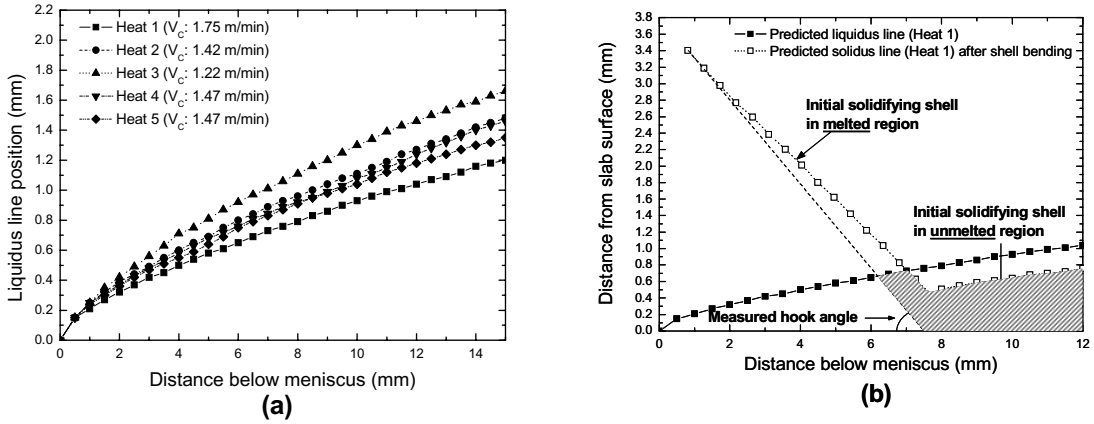

Figure 16 a) Liquidus line predicted by CON1D and b) influence on liquidus line on hook shape (Heat 1)

Figure 17 a) compares the hook lengths predicted by this method with the average measured hook length for each heat. The two values are of the same magnitude and trend, the scatter indicates that other important effects are neglected in this simple model. Therefore the difference of predicted and measured hook length was compared with superheat, classified by oscillation pitch deviation as shown in Figure 17 b). Increasing superheat and decreasing oscillation mark pitch deviation causes better agreement between the model and measurement. Worse deviation at low superheat is observed, perhaps

because hooks can survive more easily beyond the liquidus. Worse error is also observed with high pitch deviations. As earlier explained, the deviation of oscillation mark pitch is related to the liquid level stability. Larger level fluctuations generate longer, deeper hooks that require more advanced models to predict [42].

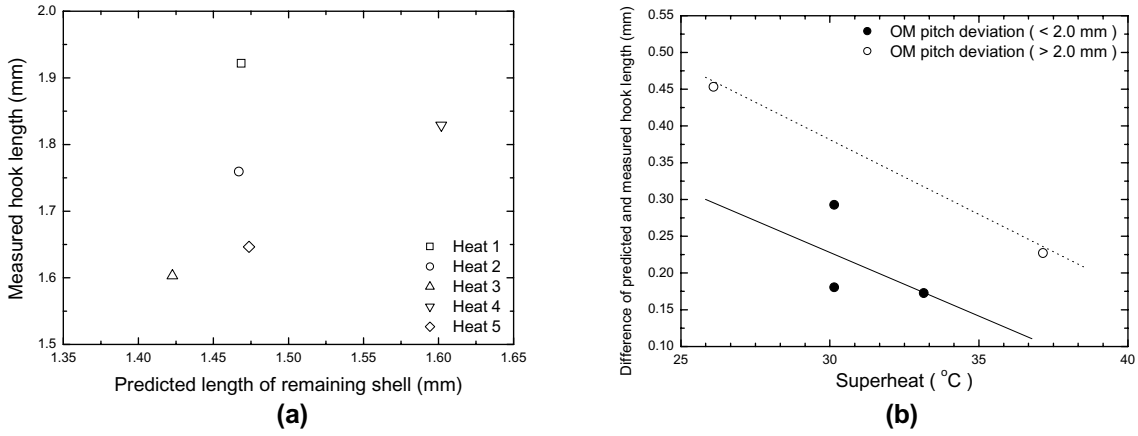

Figure 17 a) Comparison of predicted and measured hooks length and b) influence of superheat and pitch deviation on the prediction error

Summary

This study of hook characteristics focuses on the effect of heat flux at meniscus region. Plant trials conducted for five different sets of operation conditions are combined with metallographic analysis of slab samples and a computational solidification heat-flow model (CON1D). Nail board tests confirm the double roll flow pattern, shape of the steel top surface and slag layer thickness. The standard deviation of oscillation mark pitch depends on mold level fluctuations, so pitch deviations can be used to monitor meniscus stability. Thermocouple measurements and cooling water heat-up are used to calibrate the CON1D model. The predicted shell thickness at the upper oscillation mark correlates with the measured thickness of over 200 hooks. Shallower hooks correlate with a thinner initial solidifying shell. During hook formation, the initial solidifying shell is melted back by the molten steel by an amount related to the local liquidus line. Hooks are smaller and easier to predict with higher superheat and smaller level fluctuations. This work confirms the importance of heat flux in the meniscus region on hook structure, shape, and depth. This study is the first step in the development of a comprehensive model to predict hook and oscillation mark formation, in order to find ways to improve surface quality.

Acknowledgement

The authors wish to thank the Continuous Casting Consortium at the University of Illinois and POSCO, Gwangyang Works, S. Korea for support and help with the plant data.

References

1. J. K. Brimacombe and K. Sorimachi, “Crack Formation in the Continuous Casting of Steel,” *Metallurgical Transactions B*, 8B (1977), 489-505.
2. K.-D. Schmidt et al., “Consequent Improvement of Surface Quality by Systematic Analysis of Slabs,” *Steel Research*, 74 (11/12) (2003), 659-666.
3. T. Emi et al., “Influence of Physical and Chemical Properties of Mold Powders on the Solidification and Occurrence of Surface Defects of Strand Cast Slabs,” *Proceedings-National Open Hearth and Basic Oxygen Steel Conference*, 61 (1978), 350-361.

4. M.M. Wolf, “Mold Oscillation Guidelines,” *Steelmaking Conference Proceedings*, 74 (1991), 51-71.

5. Jean-Pierre et al., “The Continuous Casting Mold: A Basic Tool for Surface Quality and Strand Productivity,” *Steelmaking Conference Proceedings*, 74 (1991), 39-50.

6. H. Nakato et al., “Improvement of Surface Quality of Continuous Cast Slabs by High Frequency Mold Oscillation,” *Steelmaking Conference Proceedings*, 68 (1985), 361-365.

7. K. Nakai et al., “Improvement of Surface Quality of Continuously Cast Slab by reducing Heat Flux Density in Mold,” Proceeding of Continuous casting 85 (London, United Kingdom: *The Institute of Metals*, 1985), 71-78.

8. R. V. Mahapatra, J. K. Brimacombe and I. V. Samarasekera, “Mold Behavior and Its Influence on Quality in the Continuous Casting of Steel Slabs: Part II. Mold Heat Transfer, Mold Flux Behavior, Formation of Oscillation Marks, Longitudinal Off-Corner Depressions, and Subsurface Cracks,” *Metallurgical Transactions B*, 22B (1991), 875-888.

9. A. Yamauchi et al., “Cooling Behavior and Slab Surface Quality in Continuous Casting with Alloy 718 Mold,” *ISIJ International*, 42 (10) (2002), No. 10, pp. 1094-1102.

10. E. Takeuchi and J. K. Brimacombe, “The Formation of Oscillation Marks in the Continuous Casting of Steel Slabs,” *Metallurgical Transactions B*, 15B (Sept.) (1984), 493-509.

11. Y. Nakamori et al., “Development of Measuring System for Friction in Continuous Casting Mold,” *Tetsu-to-Hagane*, 70 (9) (1984), 1262-1268.

12. J. Savage and W. H. Pritchard, “Problem of Rupture of Billet in Continuous Casting of Steel,*” Iron and Steel Institute*, 178 (Part 3) (1954), 269-277.

13. E. S. Szekeres, “Overview of Mold Oscillation in Continuous Casting,*” Iron and Steel Engineer*, 73 (7) (1996), 29-37.

14. I. G. Saucedo, “Early Solidification during the Continuous Casting of Steel,” *Steelmaking Conference Proceedings*, 74 (1991), 79-89.

15. R. S. Laki, J. Beech and G. J. Davies, “Curved-Boundary Heat Transfer Model and its Application to Meniscus Zone during Casting,*” Ironmaking and Steelmaking*, 11 (1984), 283-291.

16. K. Bo et al., “Mechanism of Oscillation Mark Formation in Continuous Casting of Steel,” *Journal of University of Science and Technology Beijing*, 7 (3) (2000), 189-192.

17. H. Yamamura, Y. Mizukami and K. Misawa, “Formation of a Solidified Hook-like Structure at the Subsurface in Ultra Low Caron Steel,” *ISIJ International*, 36 (1996, Supplement), S223-226.

18. M. M. Wolf and W. Kurz, “Solidification of Steel in Continuous Casting Molds,” *Solidification and Casting of Metals* (Sheffield, United Kingdom; The Metals Society, 1977), 287-294.

19. M. M. Wolf, “Solidification Control in Continuous Casting of Steel,” *Solidification Processing 1987* (Sheffield, United Kingdom: The Institute of Metals, 1987), 182-186.

20. Y. Kitano et al., “Improvement of Slab Surface Quality of Ultra Low Carbon Steel,” *Tetsu-to-Hagane*, 80 (1994), T165-168.

21. M. Suzuki et al., “Initial Solidification Behavior of Ultra Low Carbon Steel,” *CAMP-ISIJ*, 11 (1998), 42-44.

22. D.W. van der Plas et al., “Combined Investigations of the EMBR Performance at Continuous Casters of Sollac Dunkerque and Hoogovens Ijmuiden,” *Proceedings 2nd European Conference on Continuous Casting*, 1 (1994), 109-118.

23. N. C. A. M. Pinheiro et al., “Mold heat transfer and continuously cast billet quality with mould flux lubrication Part 2 Quality issues,” *Ironmaking and Steelmaking*, 27 (2) (2000), 144-159.

24. I. V. Samarasekera, R. Bommaraju and J. K. Brimacombe, “Mould Heat Transfer and Solidification in the Continuous Casting of Steel Billets,” *Electric Furnace Conference Proceedings*, 1985, 249-274.

25. B. G. Thomas, "Fluid Flow in the Mold", *Chapter 14 in Making, Shaping and Treating of Steel*, ed. A. Cramb (Pittsburgh, PA: AISE Steel Foundation, 2003), 14.1-14.41.

26. M. Nadif et al., “Influence of Shell Solidification on Generation of Slab Defects-Use of Hydraulic Mold Oscillation at Sollac Florange,*” La Metllurgia Italiana*, 84 (1992), 419-424.

27. O. Pütz, O. Vreitfeld and S. Rödl, “Investigations of Flow Conditions and Solidification in Continuous Casting Moulds by Advanced Simulation Techniques,” *Steel Research*, 74 (11/12) (2003), 686-692.

28. Y. Meng and B. G. Thomas, "Heat-Transfer and Solidification Model of Continuous Slab Casting: CON1D," *Metallurgical and Materials Transactions B*, 34B (5) (2003), 685-705.

29. Y.-M. Won and B. G. Thomas, "Simple Model of Microsegregation during Solidification of Steels," *Metallurgical and Materials Transactions A,* 32A (July) (2001), 1755-1767.

30. P. V. Riboud et al., "Improvement of Continuous Casting Powders," *Fachberichte Huttenpraxis Metallweiterverarbeitung*, 19 (8) (1981), 859-869.

31. Y. Meng and B. G. Thomas, "Modeling Transient Slag-Layer Phenomena in the Shell/Mold Gap in Continuous Casting of Steel," *Metallurgical and Materials Transactions,* Vol. 34, No. 5, 2003, pp. 707-725.

32. J. K. Park, B. G. Thomas and I. V. Samarasekera, "Thermal and Mechanical Behavior of Copper Molds during Thin-Slab Casting (I): Plant Trial and Mathematical Modeling," *Materials Transactions B*, 33B (3) (2002), 425-436.

33. B. G. Thomas et al., "Optimisation of Narrow Face Water Slot Design for Siderar Slab Casting Mould," Ironmaking and Steelmaking, 30 (3) (2003), 235-239.

34. J. W. Cho et al., "Heat Transfer across Mold Flux Film in Mold during Initial Solidification in Continuous Casting of Steel," *ISIJ International*, 38 (8) (1998), 834-842.

35. M. Suzuki, M. Suzuki and M. Nakada, "Perspectives of Research on High-speed Conventional Slab Continuous Casting of Carbon Steels," *ISIJ International*, 41 (7) (2001), 670-682.

36. A.W. Cramb and F. J. Mannion, "The Measurement of Meniscus Marks at Bethlehem Steel's Burns Harbor Slab Caster," *Steelmaking Conference Proceedings*, 68 (1985), 349-359.

37. D. K. Stemple, E. N. Zulueta and M. C. Flemings, "Effect of Wave Motion on Chill Cast Surfaces," *Materials Transactions B*, 13B (3) (1982), 503-509.

38. H.-J. Shin et al., "Effect of Mold Oscillation on Powder Consumption and Hook Formation in Ultra Low Carbon Steel Slabs," (Paper will be presented at AISTech 2004, Nashville, Tennessee, 16 September, 2004)

39. C. Genzano et al., "Elimination of Surface Defects in Cold-Rolled Extra Low Carbon Steel Sheet," Iron and Steelmaker, 29 (6) (2002), 23-26.

40. M. Suzuki et al., "Development of a New Mold Oscillation Mode for High-speed Continuous Casting of Steel Slabs," *ISIJ International*, 31 (3) (1991), 254-261.

41. S. Takeuchi et al., "Control of Oscillation Mark Formation during Continuous Casting," *Steelmaking Conference Proceedings*, 74 (1991), 37-41.

42. B.G. Thomas and H. Zhu, "Thermal Distortion of Solidifying Shell in Continuous Casting of Steel," *Solidification Science and Processing*, ed. I. Ohnaka and D.M. Stefanescu, (Warrendale, PA, TMS, 1996), 197-208.